

Effects of Support Composition and Pretreatment Conditions on the Structure of Vanadia Dispersed on SiO₂, Al₂O₃, TiO₂, ZrO₂, and HfO₂

Bryan Olthof, Andrei Khodakov, Alexis T. Bell,^{*,†} and Enrique Iglesia^{*,‡}

Chemical Sciences Division and Material Sciences Division, Lawrence Berkeley National Laboratory, and Department of Chemical Engineering, University of California, Berkeley, California 94720-1462

Received: June 24, 1999; In Final Form: September 24, 1999

Spectroscopic techniques (X-ray absorption, Raman, and UV–visible) were utilized to monitor the effect of adsorbed water, calcination temperature, and reduction in H₂ on the structure of dispersed VO_x for vanadia supported on SiO₂, Al₂O₃, TiO₂, ZrO₂, and HfO₂ prepared with VO_x surface densities ranging from 0.46 VO_x/nm² to 11.1 VO_x/nm². Supported vanadia was found to exist as monovanadate, polyvanadate, or V₂O₅ species, the distribution among these species depending on the support for a given VO_x surface density. Dehydration resulted in the appearance of monovanadate species on all supports, with the extent of these species decreasing in the order HfO₂ > Al₂O₃ > ZrO₂ > TiO₂ > SiO₂. Hydration of the samples caused a decrease in the monovanadate species and a slight increase in polyvanadate species. Oxidation at elevated temperature resulted in an increase in the crystallinity of V₂O₅ present on SiO₂, a conversion of V₂O₅ into polyvanadate species on Al₂O₃, and the appearance of mixed-metal oxide phases on TiO₂, ZrO₂ (ZrV₂O₇), and HfO₂ (HfV₂O₇). The appearance of an interaction between vanadia and titania coincides with the transformation from anatase to rutile TiO₂. ZrV₂O₇ and HfV₂O₇ are postulated to form via the interaction of surface VO_x species with the support as the support begins to undergo a phase transition from tetragonal to monoclinic. H₂ reduction produced limited changes in the structure of dispersed vanadia except on Al₂O₃, where V₂O₅ was transformed into polyvanadate species.

Introduction

Supported vanadium oxide catalysts are active and selective for several partial oxidation reactions, including the selective reduction of NO_x with ammonia and the oxidative dehydrogenation of alkanes.^{1–3} The catalytic properties of these catalysts depend on the structure of the supported vanadium species.^{2,3} Depending on the support material and the VO_x concentration, supported vanadium oxide can exist as isolated tetrahedral monovanadates, one- or two-dimensional polyvanadate domains, or bulk V₂O₅ crystallites.³

Isolated monovanadate structures have been detected at low vanadium coverage on SiO₂, Al₂O₃, TiO₂, ZrO₂, and HfO₂ supports.^{2–4} VO_x species condense into chains or two-dimensional domains and ultimately into bulk V₂O₅ crystallites as VO_x loading increases.⁵ ⁵¹V NMR and Raman spectroscopy show that V⁵⁺ centers evolve from tetrahedral coordination at low coverage to octahedral coordination at higher coverage on Al₂O₃ and TiO₂.^{5,6} Also the structure of dispersed vanadia changes upon exposure to water vapor.^{4,7–12} Since water is a product of oxidation reactions, the structure of the catalyst under reaction conditions may differ from that in dehydrated samples.

The extent to which water affects the structure of dispersed vanadia depends on the composition of the support and on the temperature at which the exposure to water occurs. SiO₂-supported vanadium is especially susceptible to structural changes upon exposure to water at room temperature. Dehydrated MCM-48 materials containing V⁵⁺ ions change color from white to orange when contacted with H₂O at room

temperature.⁷ ⁵¹V NMR and Raman and UV–visible spectroscopies detect changes in SiO₂-supported V⁵⁺ coordination number from four in the dehydrated state to six in the hydrated state.^{7,8,11,12} At room temperature, water has little effect on VO_x/Al₂O₃ and VO_x/TiO₂ structure.^{4,8} At higher temperature (> 393 K), water does not cause detectable changes in VO_x/SiO₂ structure, but its effect on VO_x/Al₂O₃ and VO_x/TiO₂ structure becomes significant.¹⁰

In the absence of water, supported VO_x catalysts undergo structural changes when oxidized at elevated temperatures. As the oxidation temperature increases for highly loaded VO_x/ZrO₂, the dispersed VO_x reacts with the support to form ZrV₂O₇.^{13–15} X-ray diffraction (XRD) experiments detect a solid–solid interaction between V₂O₅ and Al₂O₃ at high temperatures^{16,17} and surface VO_x have been reported to migrate into TiO₂ to form a mixed-metal oxide.^{18–20}

This work addresses three issues concerning the structure of vanadia supported on SiO₂, Al₂O₃, TiO₂, ZrO₂, and HfO₂. The first is the effect of hydration–dehydration, the second is the effect of calcination temperature, and the third is the effect of reduction and reoxidation. Raman spectroscopy is used in order to monitor structural changes in the dispersed vanadia as a function of pretreatment conditions. UV–visible spectroscopy is used to detect changes in the domain size of the dispersed vanadia, as this technique has proven to be effective for characterizing the dispersion of metal oxides.^{21,22} Information about the local structure of V⁵⁺ cations in dispersed vanadia is obtained from X-ray absorption spectra.

Experimental Section

Catalyst samples were prepared via incipient wetness impregnation of support materials with aqueous NH₄VO₃ solutions

* To whom correspondence should be addressed. E-mail: bell@cchem.berkeley.edu; iglesia@cchem.berkeley.edu.

[†] Chemical Sciences Division.

[‡] Material Sciences Division.

TABLE 1: Vanadium Content, Surface Area, and Calculated VO_x Surface Density for Supported Vanadium Oxide Catalysts Studied

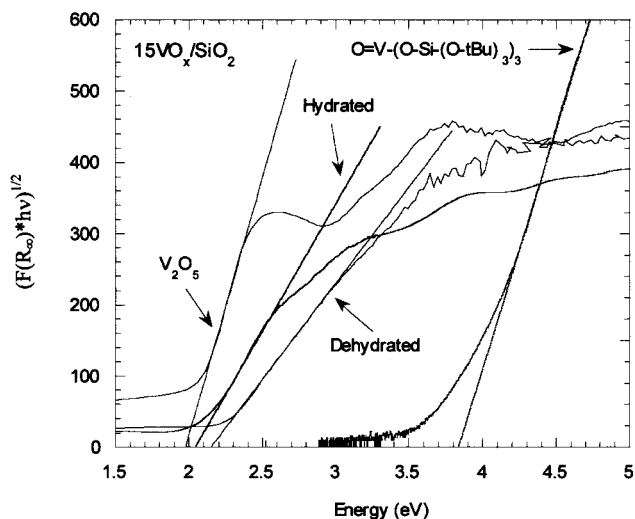
support	catalyst	V ₂ O ₅ content (wt %)	BET surface area (m ² /g)	VO _x surface density (VO _x /nm ²)
Al ₂ O ₃	0.7VO _x /Al ₂ O ₃	0.7	88	0.5
	2VO _x /Al ₂ O ₃	2	100	1.3
	3.5VO _x /Al ₂ O ₃	3.5	100	2.3
	5VO _x /Al ₂ O ₃	5	96	3.5
	10VO _x /Al ₂ O ₃	10	89	7.7
SiO ₂	15VO _x /Al ₂ O ₃	15	86	12.0
	2VO _x /SiO ₂	2	287	0.46
	5VO _x /SiO ₂	5	283	1.2
TiO ₂	10VO _x /SiO ₂	10	271	2.4
	15VO _x /SiO ₂	15	251	4.0
	0.7VO _x /TiO ₂	0.7	73.5	0.63
ZrO ₂	2VO _x /TiO ₂	2	69.0	1.9
	3.5VO _x /TiO ₂	3.5	69.5	3.3
	5VO _x /TiO ₂	5	58	5.7
	2VO _x /ZrO ₂	2	144	0.92
	5VO _x /ZrO ₂	5	155	2.1
HfO ₂	10VO _x /ZrO ₂	10	170	3.9
	15VO _x /ZrO ₂	15	160	6.2
	1.2VO _x /HfO ₂	1.2	62	1.3
	3VO _x /HfO ₂	3	79	2.5
	6.1VO _x /HfO ₂	6.1	125	3.2
	9.4VO _x /HfO ₂	9.4	115	5.4

(99%, Aldrich, Inc.). Oxalic acid was added to these solutions (Mallinckrodt, analytical grade; NH₄VO₃/oxalic acid = 0.5 molar) in order to ensure complete dissolution of ammonium metavanadate precursors. SiO₂ (Davison Chemical), Al₂O₃ (Degussa, AG), and TiO₂ (Sud-Chemie, AG) supports were obtained from commercial sources. Zirconium (ZrO(OH)₂) and hafnium (HfO(OH)₂) oxyhydroxides were prepared by coprecipitation at pH 10 from the corresponding oxychlorides.² After impregnation, samples were dried overnight in air at 393 K and treated in flowing dry air at 773 K for 3 h. OV[OSi(O^tBu)₃]₃²³ was used as a reference compound for UV-visible and X-ray absorption studies, to characterize isolated tetrahedrally coordinated vanadyl groups.

Surface areas were measured in a N₂ physisorption flow apparatus using thermal conductivity detection and multipoint BET analysis methods. Samples were dehydrated in He at 473 K for 1 h before surface area measurements.

Diffuse reflectance UV-visible spectra were obtained with a Varian-Cary 4 spectrophotometer equipped with a Harrick diffuse-reflectance attachment, using MgO as a reference. Catalyst samples were placed in a cell equipped with a heater, water-cooling system, thermocouple, and gas flow system for in situ characterization. Spectra of hydrated samples were measured at ambient conditions. These samples were then dehydrated by treatment in flowing dry air at 723 K for 1 h. Dehydrated samples were cooled to room temperature in flowing dry air before obtaining spectra.

X-ray absorption measurements were carried out at the Stanford Synchrotron Radiation Laboratory using beamline 2-3. Dehydration was carried out in a cell equipped with a thin (1 mm) quartz capillary to contain the catalyst.²⁴ The capillary is connected to a gas manifold and is surrounded by a heater so that the sample can be treated in situ at temperatures of up to 773 K. The absorption spectrum was measured at the K edge of vanadium (5463 eV) in the fluorescence mode using a double crystal (Si₁₁₁) monochromator.²⁵ Two ion chambers were employed for X-ray detection. The first was filled with He and placed before the cell in order to measure the intensity of the beam before absorption. A second chamber, filled with Ar and

**Figure 1.** UV-visible spectra of 15VO_x/SiO₂ before and after dehydration.

situated at a 90° angle incident from the X-ray beam, was used to measure the fluorescence emission from samples.

Raman spectra were obtained using a HoloLab 5000 Research Raman spectrometer (Kaiser Optical Systems, Inc.) with a 532 nm solid-state laser (Coherent Laser Group). Backscattered light was measured with a thermoelectrically cooled CCD detector (Princeton Instruments, Inc.). Spectra were acquired over the range 0–4000 cm⁻¹ using 50 mW and a spectral collection time of 5 min or less. Catalyst samples (~0.1 g) were pressed at 70 MPa into 9 mm diameter by 1 mm thick wafers. Wafers were placed on a rotating stage within a reactor fitted with a Suprasil quartz optical window. The stage was mounted on the end of a ceramic rod fitted to a magnetically coupled rotary motion feedthrough device (Huntington Mechanical Laboratories). Rotation speed was controlled between 20 and 500 rpm with a power supply and step motor driver (Applied Motion Products). The reactor could be heated to 973 K using two 150 W semicylindrical radiant ceramic heaters (Omega Engineering, Inc.). The reactor was attached to a gas manifold in order to allow in situ characterization. Gases were obtained from Bay Airgas (He, 99.999%; O₂, 99.994%; H₂, 99.999%) and purified using 13X molecular sieve traps (Matheson 451).

Results

Effects of Hydration and Dehydration. Table 1 provides a summary of vanadia weight loading, catalyst surface area, and calculated VO_x surface density for all catalysts studied.² UV-visible spectra of hydrated and dehydrated 15VO_x/SiO₂ are shown in Figure 1; they are representative of the data recorded for all samples. Included in Figure 1 are spectra of bulk V₂O₅ and of OV(OSi(O^tBu)₃)₃, which provide reference absorption edge energy values for V⁵⁺ species in extended square pyramidal structures and in isolated tetrahedral environments, respectively. The calculation of absorption edge follows the procedure described in detail by Barton et al.²⁶ Reflectance data are converted into absorption spectra through the Kubelka–Munk function $F(R_{\infty})$. Absorption edge energies are then calculated by extrapolating to zero energy a linear least-squares fit of the low-energy section of a graph of $(F(R_{\infty})hv)^{1/2}$ versus hv , in accordance with the procedure for amorphous semiconductors with indirect electronic transitions.^{26–28} The spectra in Figure 1 are plotted as $(F(R_{\infty})hv)^{1/2}$ versus hv and they are shown with the linear fit of the low-energy edge. Charge transfer bands in Al₂O₃, SiO₂, HfO₂, and ZrO₂ occur at much higher energies

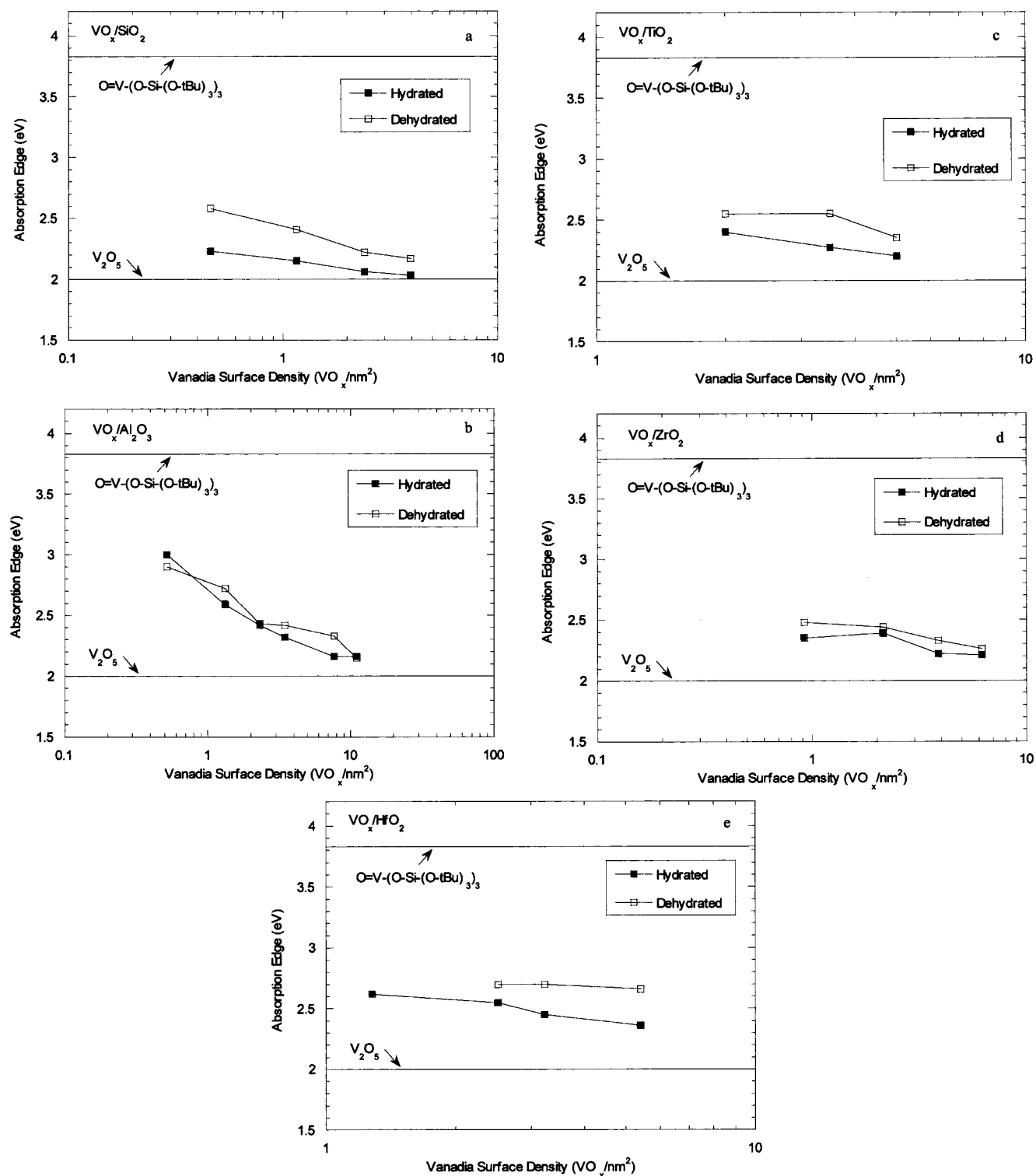


Figure 2. Absorption edge energies measured for hydrated and dehydrated vanadium catalysts: (a) VO_x/SiO_2 ; (b) $\text{VO}_x/\text{Al}_2\text{O}_3$; (c) VO_x/TiO_2 ; (d) VO_x/ZrO_2 ; (e) VO_x/HfO_2 .

than for VO_x species, and they do not interfere with the analysis of the absorption edge regions of VO_x centers. The charge transfer band of TiO_2 (3.17 eV) does overlap with bands corresponding to VO_x species. To calculate the contribution of V^{5+} species to the UV–visible spectrum, a pure TiO_2 spectrum was subtracted from that of VO_x/TiO_2 samples.²

Values of the absorption edge for hydrated and dehydrated samples are given in Figure 2. Edge energies for all hydrated samples decrease as VO_x surface density increases, consistent with the growth in domain size expected as more vanadia is

deposited on the surface.^{21,22} Dehydration of all catalysts leads to an increase in the absorption edge energy, indicating a decrease in vanadium domain size or a change in the coordination of the vanadium cations. The magnitude of this shift depends on the support material and the surface density of VO_x species. On SiO_2 -supported samples, an edge shift of 0.4 eV is observed upon dehydration at the lowest vanadia loading, and this shift decreases with increasing VO_x surface density. On Al_2O_3 and ZrO_2 supported samples, the edge shift shows no discernible trend with VO_x loading and all shifts are smaller

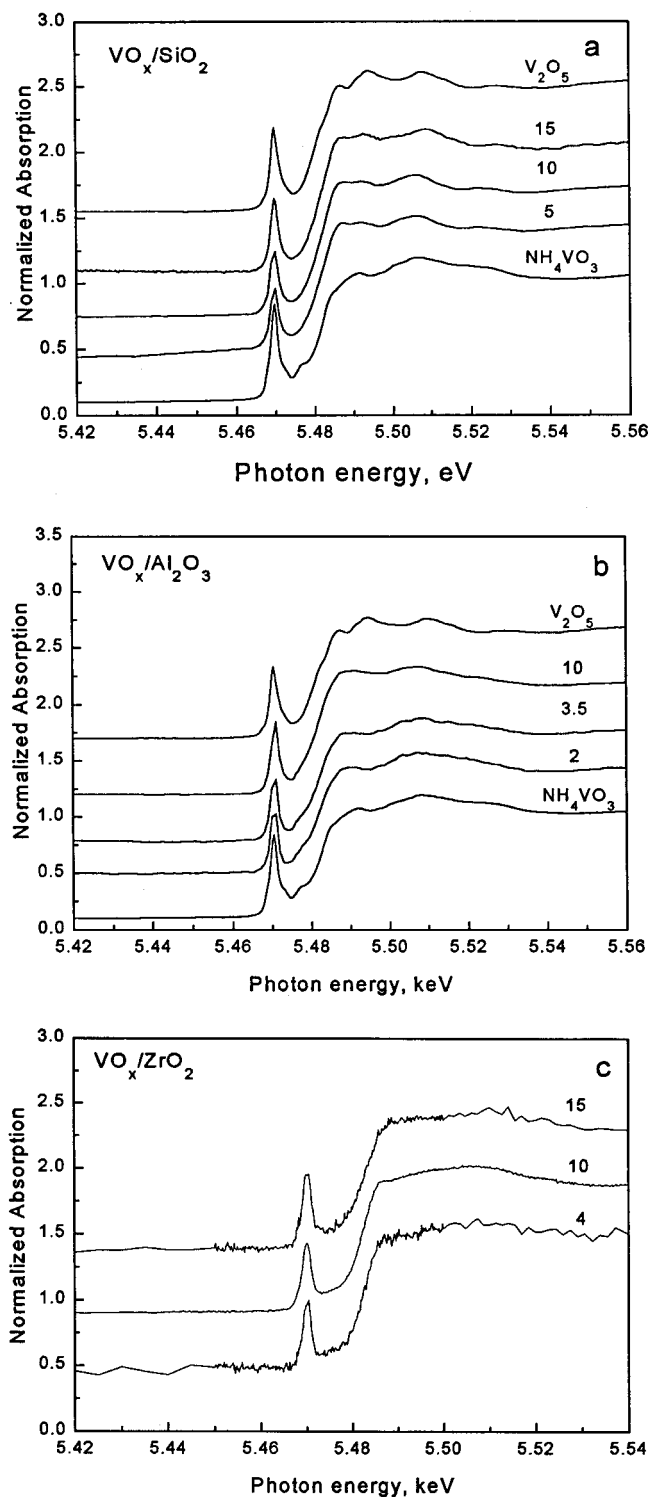


Figure 3. XANES spectra of (a) VO_x/SiO_2 , (b) $\text{VO}_x/\text{Al}_2\text{O}_3$, and (c) VO_x/ZrO_2 catalysts at ambient conditions.

than 0.2 eV. On HfO_2 supported samples, the edge shift following dehydration increases with VO_x loading, reaching a maximum of 0.3 eV at the highest surface density studied. After in situ characterization, exposure of catalyst samples to ambient air for 2 h restores the UV–visible spectra to that of the hydrated samples. Identical treatments of bulk V_2O_5 do not lead to detectable changes in the UV–visible spectra.

Near-edge X-ray absorption spectra of hydrated VO_x/SiO_2 , $\text{VO}_x/\text{Al}_2\text{O}_3$, and VO_x/ZrO_2 are shown in Figure 3. The position of edge and pre-edge features reflects the local coordination of

vanadium atoms.²⁹ Included in Figure 3b are near-edge spectra of V_2O_5 and NH_4VO_3 , compounds with known V^{5+} coordination. The near-edge spectra of all hydrated SiO_2 -supported catalysts are nearly identical, and they resemble the spectrum of V_2O_5 . It appears that, at all VO_x surface densities, vanadium coordination in hydrated VO_x/SiO_2 resembles that in V_2O_5 (square pyramidal V^{5+}). As VO_x surface density increases, the near-edge spectrum of hydrated $\text{VO}_x/\text{Al}_2\text{O}_3$ shifts from one resembling that of NH_4VO_3 (tetrahedral V^{5+}) to one resembling V_2O_5 (square pyramidal V^{5+}). The near-edge spectra of all hydrated VO_x/ZrO_2 catalysts are similar and resemble the spectrum of NH_4VO_3 more than that of V_2O_5 , suggesting that tetrahedral VO_x species remain even after exposure to H_2O at room temperature.

Near-edge spectra of hydrated and dehydrated catalysts with similar VO_x surface density (4–7.7 VO_x/nm^2) are shown in Figure 4. Dehydration leads to a shift in the K-edge spectra from that resembling V_2O_5 to that representative of isolated vanadyl species such as those found in the compound NH_4VO_3 . This effect is more pronounced for SiO_2 and Al_2O_3 supported vanadia than for ZrO_2 or HfO_2 supported vanadia.

Raman spectra of hydrated and dehydrated samples with similar VO_x surface density (4–7.7 VO_x/nm^2) are shown in Figure 5. All spectra were acquired while the sample was rotated at ~ 400 rpm in order to limit dehydration caused by laser heating. All samples, except for $5\text{VO}_x/\text{TiO}_2$, show Raman bands near 144, 285, 407, 486, 525, 699, and 995 cm^{-1} typical of V_2O_5 crystallites.^{2,4,13,30,31} None of the hydrated samples produce a clear monovanadate band, normally present around 1020–1040 cm^{-1} .^{2,10}

Hydrated $15\text{VO}_x/\text{SiO}_2$ exhibits a shoulder at 1020 cm^{-1} arising, perhaps, from partial dehydration and formation of monovanadate species due to laser heating. The sample also produces a very weak, broad band centered at 900 cm^{-1} , suggesting the presence of $\text{V}=\text{O}$ bonds in polymeric vanadia domains.^{2,4,9,12,13,32,33} Upon dehydration, the peaks assigned to V_2O_5 become narrower and more intense and a sharp peak at 1039 cm^{-1} , assigned to $\text{V}=\text{O}$ stretching in monovanadate species, appears. A band is also observed at 1060 cm^{-1} . This feature has been reported previously¹² but cannot be assigned unambiguously.

Hydrated $10\text{VO}_x/\text{Al}_2\text{O}_3$ shows a weak, broad band centered on 828 cm^{-1} , as well as a shoulder on the low wavenumber side of the V_2O_5 peak at 994 cm^{-1} . The latter peak can be assigned to $\text{V}=\text{O}$ stretching in polyvanadate structures, but the former might be attributable to either $\text{V}-\text{O}-\text{V}$ or $\text{V}-\text{O}-\text{M}$ stretching modes in polymeric vanadia.^{2,4,9,12,13,32,33} Following dehydration, a peak appears at 1032 cm^{-1} , indicating the evolution of isolated monovanadate species, while a broad feature in the 800–1000 cm^{-1} region suggests the presence of polyvanadate domains. No significant changes in V_2O_5 peaks are detected upon dehydration.

Hydrated $5\text{VO}_x/\text{TiO}_2$ produces two poorly resolved bands centered at about 800 and 900 cm^{-1} , indicating the presence of polyvanadate species.^{2,4,9,12,13,32,33} Raman intensity in the region of 800 cm^{-1} may also be due to second-order scattering from TiO_2 ($2 \times 400 \text{ cm}^{-1}$). Upon dehydration, the broad polyvanadate bands remain, but the band centered near 900 cm^{-1} becomes less intense. The appearance of a peak at 1022 cm^{-1} indicates the formation of monovanadate species. Four peaks at 149, 395, 511, and 639 cm^{-1} attributable to anatase TiO_2 do not change throughout hydration–dehydration cycles.^{4,13}

Hydrated $15\text{VO}_x/\text{ZrO}_2$ and $9.4\text{VO}_x/\text{HfO}_2$ exhibit broad Raman bands in the region of 750–1000 cm^{-1} typical of polyvanadate

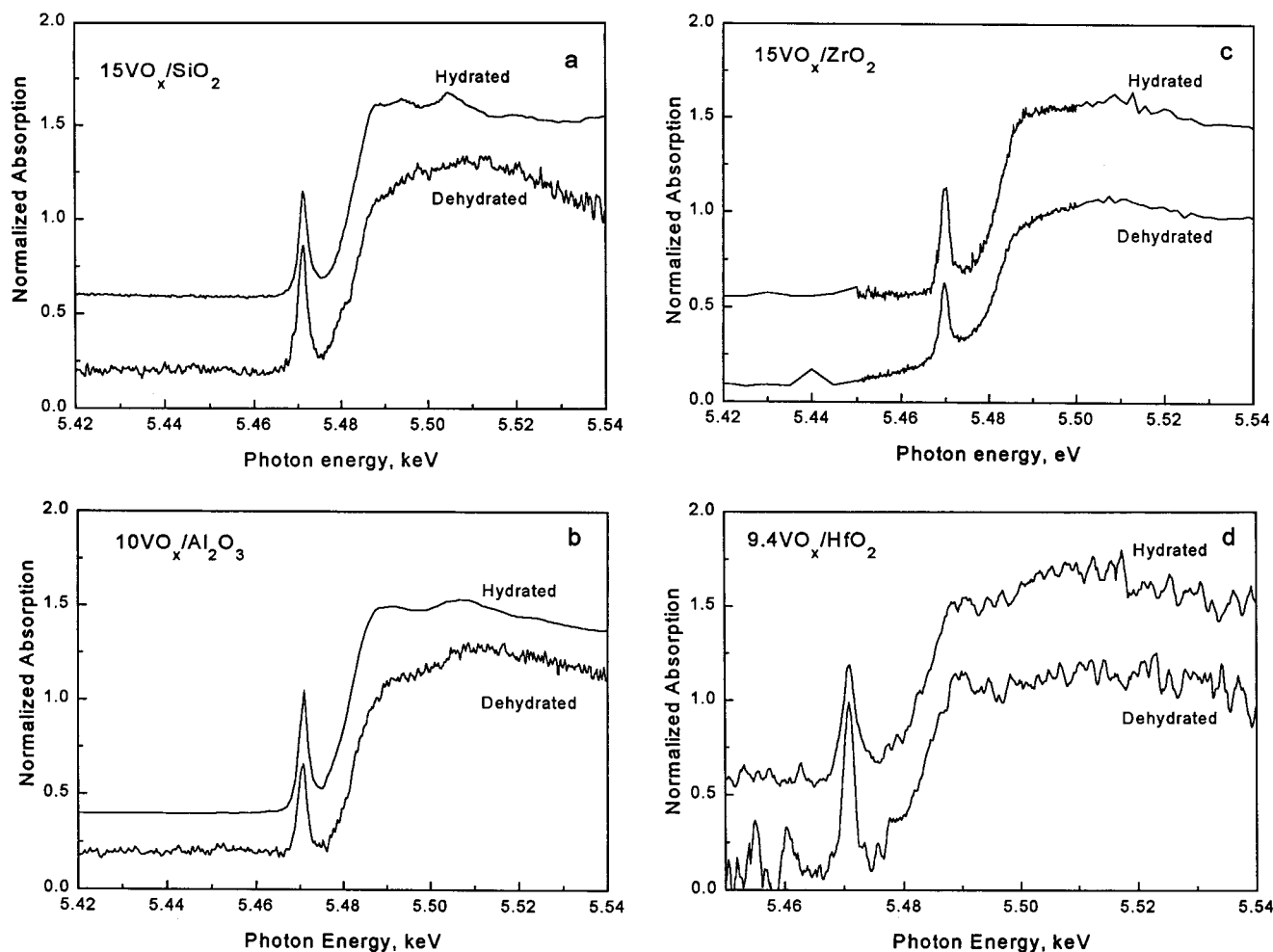


Figure 4. XANES spectra before and after dehydration for (a) $15\text{VO}_x/\text{SiO}_2$, (b) $10\text{VO}_x/\text{Al}_2\text{O}_3$, (c) $15\text{VO}_x/\text{ZrO}_2$, and (d) $9.4\text{VO}_x/\text{HfO}_2$.

species. The ZrO_2 supported catalyst exhibits a peak at 772 cm^{-1} attributable to ZrV_2O_7 and the HfO_2 supported sample exhibits an analogous peak at 800 cm^{-1} assigned to HfV_2O_7 .² Upon dehydration, V_2O_5 peaks in both samples decrease in intensity relative to the polyvanadate and $(\text{Zr}/\text{Hf})\text{V}_2\text{O}_7$ peaks. The center of each polyvanadate peak shifts to a slightly higher frequency (906 to 926 cm^{-1} on ZrO_2 ; 923 to 940 cm^{-1} on HfO_2). The concurrent appearance of a Raman band attributable to $\text{V}=\text{O}$ stretching in monovanadate species and the observed strengthening of $\text{V}=\text{O}$ bonds in polyvanadate species upon dehydration suggest that these bonds are the most susceptible to hydration.

Effects of Oxidation and Reduction. The effects of treating supported vanadia in air at progressively higher temperatures and the influence of reduction in H_2 at 723 K were investigated using samples with a vanadia surface density between 4 and $7.7\text{ VO}_x/\text{nm}^2$, corresponding to approximately 0.5 to 1.0 polyvanadate monolayers.^{14,34,35}

$15\text{VO}_x/\text{SiO}_2$ ($3.95\text{ VO}_x/\text{nm}^2$). Raman spectra of $15\text{VO}_x/\text{SiO}_2$ taken in flowing 10% O_2/He at 723 , 823 , and 923 K are shown in Figure 6, top. High surface area, amorphous SiO_2 is a poor Raman scatterer, and no peaks attributable to $\text{Si}-\text{O}$ stretches are detected.³⁵ Peaks at 143 , 282 , 406 , 489 , 524 , 694 , and 993 cm^{-1} indicative of V_2O_5 are present in the spectra acquired at 723 and 823 K . These two spectra also show a peak at 1035 cm^{-1} characteristic of $\text{V}=\text{O}$ stretching in monovanadate species.³⁶ These results are consistent with previous studies which report that vanadia interacts weakly with SiO_2 and tends to form coexisting monovanadate species and crystalline V_2O_5 at high

weight loadings without the intermediate formation of two-dimensional polyvanadate domains.^{3,4,36} The only significant change is seen in the Raman spectrum taken at 923 K . At this temperature, near the melting point of V_2O_5 (963 K), peaks attributable to $\text{V}-\text{O}-\text{V}$, $\text{V}=\text{O}$, and $\text{V}-\text{O}$ stretches in V_2O_5 completely disappear and the monovanadate peak shifts to 1018 cm^{-1} .

UV-visible absorption edges for the SiO_2 supported sample (Table 3) are present at 2.1 and 2.8 eV after oxidation at 723 K for 1 h . This suggests that the V_2O_5 detected by Raman exists in different domain sizes, perhaps as bulk V_2O_5 and as a monolayer-type sheet of V_2O_5 . Only one UV-visible absorption edge remains after treatment in air at 923 K . The edge at 2.0 eV , which is equivalent to that of V_2O_5 , suggests that amorphous vanadia, as well as monovanadate species, condense into a six-coordinate overlayer structure resembling bulk V_2O_5 on SiO_2 when silica-supported vanadia is treated at temperatures high enough to allow surface rearrangement. Raman results support this proposal. The middle panel of Figure 6 compares Raman spectra taken at 298 K of $15\text{VO}_x/\text{SiO}_2$ after oxidation at 723 and 923 K . V_2O_5 peaks that were absent in spectra acquired at 923 K (Figure 6, top) reappear after cooling and are higher in intensity and sharpness than V_2O_5 peaks produced by the sample oxidized at 723 K . One particular difference is the increase in intensity of the peak $\sim 510\text{ cm}^{-1}$ which has previously been assigned to $\text{V}-\text{O}-\text{V}$ stretching in V_2O_5 .³⁰

After oxidation at 723 K ($100\text{ cm}^3/\text{min}$ of 10% O_2/He for 1 h), the SiO_2 supported sample was exposed to cycles of

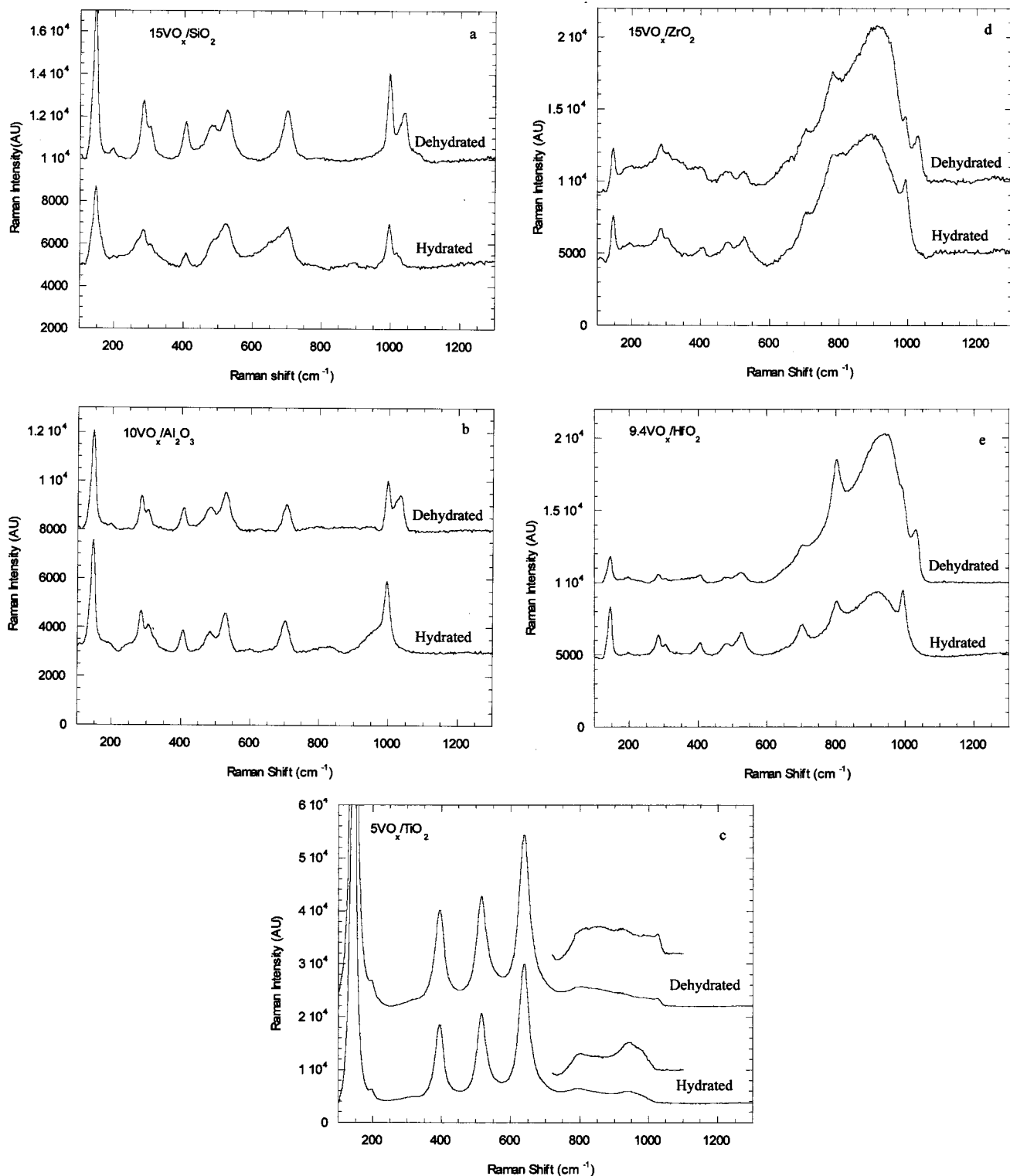


Figure 5. Raman spectra for (a) $15\text{VO}_x/\text{SiO}_2$, (b) $10\text{VO}_x/\text{Al}_2\text{O}_3$, (c) $5\text{VO}_x/\text{TiO}_2$, (d) $15\text{VO}_x/\text{ZrO}_2$, and (e) $9.4\text{VO}_x/\text{HfO}_2$ before and after dehydration.

reduction (100 cm^3/min of 10% H_2/He for 2 h) and oxidation (100 cm^3/min of 10% O_2/He for 3 h) at 723 K. Raman spectra of the sample taken in dry He at 373 K after each treatment are shown in Figure 6, bottom panel. Peaks corresponding to V_2O_5 sharpen upon reduction and the monovanadate peak at 1035 cm^{-1} decreases in intensity relative to the V_2O_5 peaks. Only one UV-visible absorption edge energy (2.9 eV) is present following reduction (Table 4). Reoxidation restores the UV-visible edge energy at 2.1 eV and increases the Raman intensity

of monovanadate peaks, indicating that structural changes induced by reduction are reversible.

$10\text{VO}_x/\text{Al}_2\text{O}_3$ ($7.7 \text{VO}_x/\text{nm}^2$). Raman spectra of $10\text{VO}_x/\text{Al}_2\text{O}_3$ taken in flowing 10% O_2/He at 723, 823, and 923 K are shown in Figure 7, top panel. $\gamma\text{-Al}_2\text{O}_3$, like SiO_2 , is a poor Raman scatterer and no peaks attributable to Al_2O_3 are observed in the spectra.³⁵ At 723 K, peaks at 140, 282, 406, 521, 696, and 993 cm^{-1} indicate the presence of V_2O_5 ; the peak at 1027 cm^{-1} indicates the presence of monovanadate units, and a weak broad

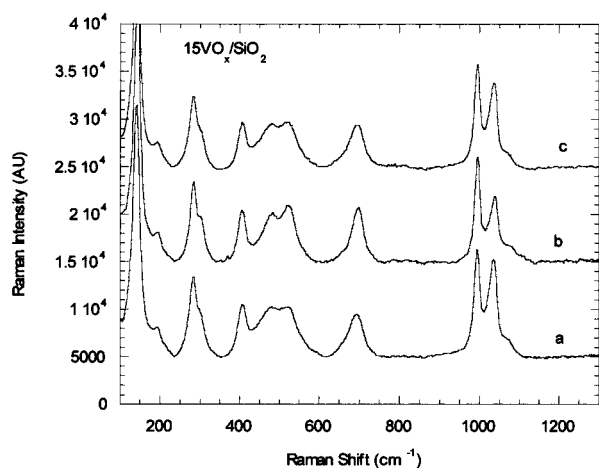
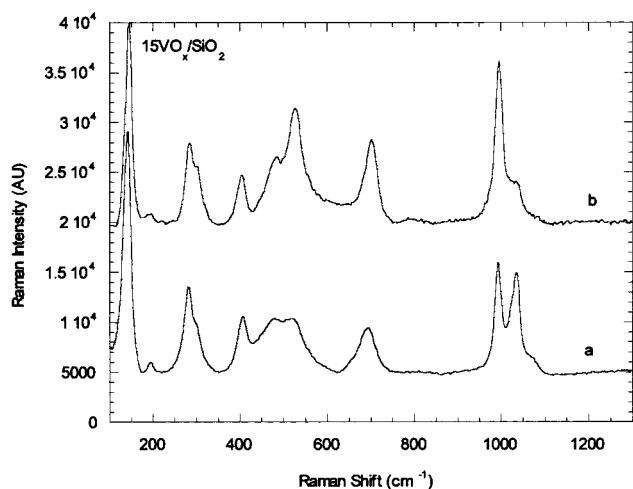
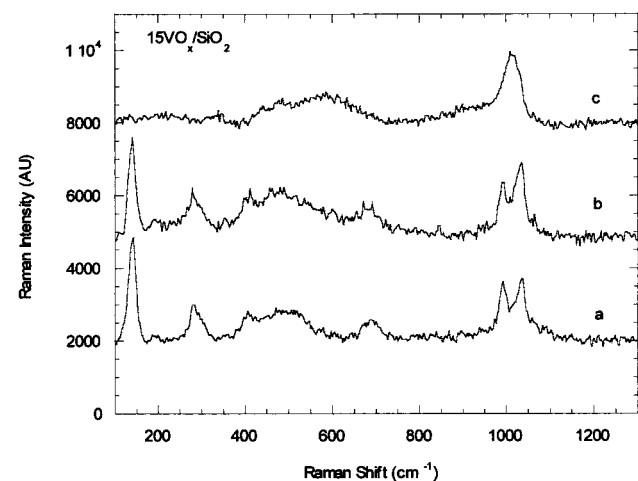


Figure 6. Raman spectra of $15\text{VO}_x/\text{SiO}_2$: (top) taken at (a) 723, (b) 823, and (c) 923 K; (middle) taken at 298 K after calcining at (a) 723 K and (b) 923 K; (bottom) taken at 298 K after (a) oxidation, (b) reduction, and (c) reoxidation at 723 K.

band in the $750\text{--}950\text{ cm}^{-1}$ region suggests the presence of polyvanadate species on the Al_2O_3 support. Upon heating to 823 and 923 K, the V_2O_5 peaks disappear while the broad polyvanadate peak separates into two peaks centered at ~ 770 and $\sim 880\text{ cm}^{-1}$.

The middle panel of Figure 7 shows that higher oxidation temperatures lead to improved vanadia dispersion on Al_2O_3 . After oxidizing at 723 K, V_2O_5 predominates on the surface,

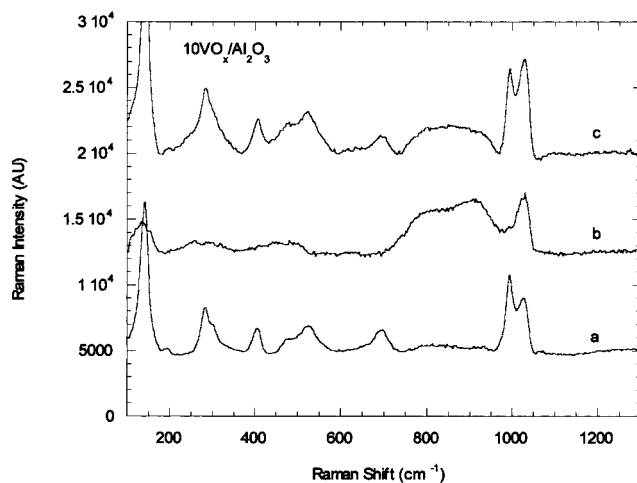
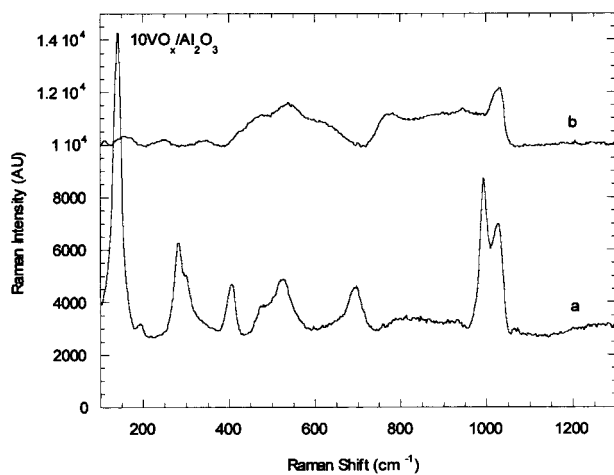
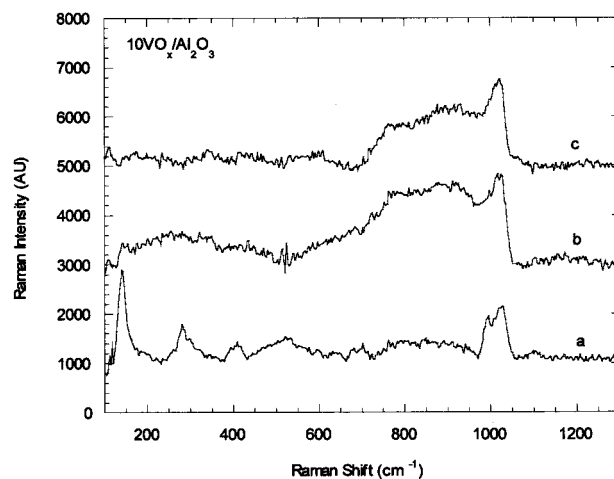


Figure 7. Raman spectra of $10\text{VO}_x/\text{Al}_2\text{O}_3$: (top) taken at (a) 723, (b) 823, and (c) 923 K; (middle) taken at 298 K after calcining at (a) 723 K and (b) 923 K; (bottom) taken at 298 K after (a) oxidation, (b) reduction, and (c) reoxidation at 723 K.

with some evidence of polyvanadate environments. Oxidizing at 923 K converts V_2O_5 species into polyvanadate arrays.

The UV–visible absorption edges for the Al_2O_3 supported sample (Table 3) are present at 2.3 and 2.5 eV after oxidation at 723 K for 1 h. The higher absorption edge energy, relative to that seen for VO_x/SiO_2 , suggests that the V_2O_5 seen in the Raman spectra of $\text{VO}_x/\text{Al}_2\text{O}_3$ exist in smaller domains than V_2O_5 on SiO_2 . Oxidizing at 923 K produces no detectable change in the UV–visible absorption spectrum (Table 3). Raman spectra

shown in the middle panel of Figure 7 clearly show, however, that the dispersed V_2O_5 changes its structure when treated at high enough temperature. On Al_2O_3 , this results in transformation of V_2O_5 into polyvanadate species, while on SiO_2 it leads to the formation of crystalline V_2O_5 overlayers, suggesting that vanadia wets the surface of Al_2O_3 more effectively than the surface of SiO_2 .

After oxidation at 723 K (100 cm^3/min of 10% O_2/He for 1 h), the $10VO_x/Al_2O_3$ sample was exposed to reduction (100 cm^3/min of 10% H_2/He for 2 h) and oxidation (100 cm^3/min of 10% O_2/He for 3 h) cycles at 723 K. Raman spectra of the sample taken in dry He at 373 K after each treatment are shown in Figure 7, bottom panel. Reduction results in the disappearance of the V_2O_5 peaks and the development of two polyvanadate peaks centered at ~ 770 and ~ 910 cm^{-1} , similar to those observed after oxidation at elevated temperatures.

V_2O_5 peaks reappear following reoxidation but the intensities of the bands for this species are less intense compared with those for monovanadate species, than in the spectrum of the freshly oxidized sample (Figure 7, bottom). The broad polyvanadate peak is also more intense than that for the freshly oxidized sample, but less intense than that for the reduced sample. This indicates that some of the polyvanadate species generated by the reduction of V_2O_5 have not reoxidized to the original V_2O_5 state. This observation could be explained by the results of Andersen and Kung, who found that reoxidation conditions have a significant effect on the extent of reoxidation for VO_x/Al_2O_3 .³⁷ Specifically, these authors found that reoxidation temperatures had to be raised above reduction temperatures to achieve full reoxidation.³⁷

$5VO_x/TiO_2$ ($5.7 VO_x/nm^2$). Raman spectra of $5VO_x/TiO_2$ taken in flowing 10% O_2/He at 723, 823, and 923 K are shown in the top panel of Figure 8. All spectra show peaks at 149, 394, 512, and 636 cm^{-1} indicative of the anatase phase of TiO_2 .^{4,13} Spectra are displayed after background subtraction in the region of 730–1100 cm^{-1} in order to amplify the portion of the spectrum arising from vanadia. At 723 K, the broad band from 800 to 1000 cm^{-1} indicates the presence of polyvanadate species and the weak band at 1022 cm^{-1} indicates the presence of isolated monovanadate units.⁴ After heating to 823 K, the peak at 1022 cm^{-1} decreases in intensity but the polyvanadate peak remains unchanged. At 923 K, the polyvanadate region separates into two bands centered at ~ 800 and ~ 915 cm^{-1} and the TiO_2 peaks decrease in relative intensity. The middle panel of Figure 8 illustrates these changes more clearly by comparing spectra taken at 298 K after treatment at 723 and 923 K. After calcining at 923 K, the polyvanadate region exhibits two separate peaks, centered at ~ 810 and ~ 930 cm^{-1} . It also appears that TiO_2 has begun a phase transition, evidenced by the broad peak at 444 cm^{-1} and a shoulder at 608 cm^{-1} attributable to rutile TiO_2 .^{13,18} The transformation of TiO_2 from anatase to rutile would explain the sharp drop in surface area after calcination at 923 K (Table 2).

The absorption edge energy for the TiO_2 supported sample (Table 3) appears at 2.3 eV after oxidation at 723 K for 1 h. Higher calcination temperatures do not produce detectable changes in the absorption edge energy.

These results agree with previous studies of VO_x/TiO_2 catalysts, which indicate that TiO_2 disperses vanadia well. Monovanadate and polyvanadate species with 5-fold coordination form on TiO_2 .^{4,38} An earlier oxidation study utilizing Raman and UV–visible spectroscopy showed the formation of vanadium–titanium mixed oxides, in which TiO_2 retains the anatase

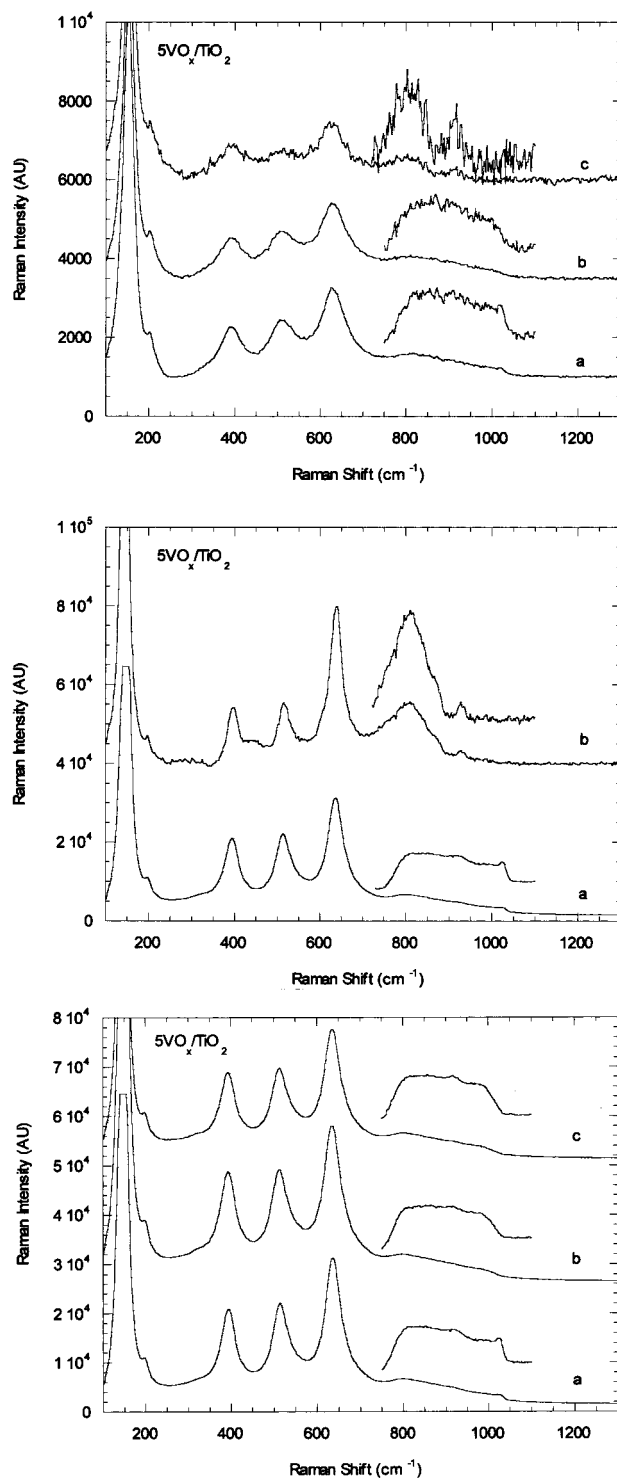


Figure 8. Raman spectra of $5VO_x/TiO_2$: (top) taken at (a) 723, (b) 823, and (c) 923 K; (middle) taken at 298 K after calcining at (a) 723 K and (b) 923 K; (bottom) taken at 298 K after (a) oxidation, (b) reduction, and (c) reoxidation at 723 K.

structure.¹⁸ Other investigators have observed the formation of a mixed oxide of vanadia with rutile TiO_2 .^{19,20} As the oxidation temperature is increased, the transition from anatase to rutile is caused by the migration of vanadia into the TiO_2 lattice. The spectra presented here show some evidence of rutile formation. The migration of vanadia into the TiO_2 lattice could explain the decrease in intensity of the monovanadate peak seen in Figure 6, but not the collapse in surface area (Table 2). Thus,

TABLE 2: BET Surface Area and VO_x Surface Density after Oxidation at 723 and 923 K

sample	calcination temperature			
	723 K		923 K	
	BET surface area (m ² /g)	VO _x surface density (VO _x /nm ²)	BET surface area (m ² /g)	VO _x surface density (VO _x /nm ²)
5VO _x /TiO ₂	58	5.7	39	8.5
15VO _x /ZrO ₂	160	6.2	35	28.3
9.4VO _x /HfO ₂	115	5.4	52	12.0
15VO _x /SiO ₂	251	4.0	215	4.6
10VO _x /Al ₂ O ₃	89	7.7	85	8.1

TABLE 3: UV–Visible Absorption Edge Energies (eV) after Oxidation at 723 and 923 K

sample	oxidation temperature	
	723 K	923 K
5VO _x /TiO ₂	2.3	2.3
15VO _x /ZrO ₂	2.3	2.2
9.4VO _x /HfO ₂	2.7	2.5
15VO _x /SiO ₂	2.1, 2.8	2.0
10VO _x /Al ₂ O ₃	2.3, 2.5	2.3, 2.5

TABLE 4: UV–Visible Absorption Edge Energies (eV) after Oxidation and Reduction at 723 K

sample	oxidized	reduced	reoxidized
5VO _x /TiO ₂	2.3	2.9	2.3
15VO _x /ZrO ₂	2.3	2.3	2.3
9.4VO _x /HfO ₂	2.7	2.7	2.6
15VO _x /SiO ₂	2.1, 2.8	2.9	2.1, 2.9
10VO _x /Al ₂ O ₃	2.3, 2.5	2.4	2.3, 2.5

it seems likely that the migration of vanadia into TiO₂ occurs concurrently with the transformation of TiO₂ from anatase to rutile.

After oxidizing at 723 K (100 cm³/min of 10% O₂/He for 1 h) the TiO₂ supported sample was subjected to reduction (100 cm³/min of 10% H₂/He for 2 h) and oxidation (100 cm³/min of 10% O₂/He for 3 h) cycles at 723 K. Raman spectra taken in dry He at 373 K after each treatment are shown in the bottom panel of Figure 8. The four peaks arising from anatase TiO₂ do not change upon reduction or reoxidation. The peak at 1022 cm⁻¹ attributed to monovanadate species in the oxidized sample is no longer present after reduction. Reoxidation does not produce significant changes in the spectrum of the reduced sample. This would suggest that hydrogen reduction either forms a stable, anatase, mixed-metal oxide or induces monovanadate polymerization. Alternatively, a VO_x-rutile TiO₂ species may be forming, but not enough TiO₂ has undergone transition to produce a detectable change in the Raman spectrum.

The UV–visible absorption edge shifts from 2.3 to 2.9 eV upon reduction by hydrogen at 723 K (Table 4), indicating a decrease in the domain size of surface vanadia species. This agrees well with the mechanism proposed by Went et al. which involves reduction of monomeric and polymeric vanadia from 5-fold to 4-fold coordination centers.³⁹ Reoxidation restores the UV–visible absorption edge to 2.3 eV, indicating that the largest vanadia domains are restored upon reoxidation. Combined with the Raman results, this suggests that after reoxidation all surface vanadia is present as extended polyvanadate domains. Vanadate species initially present as tetrahedral monovanadate units have either migrated into the TiO₂ or polymerized to form polyvanadate domains.

15VO_x/ZrO₂ (6.2 VO_x/nm²). Raman spectra of 15VO_x/ZrO₂ taken under flowing 10% O₂/He at 723, 823, and 923 K are shown in the top panel of Figure 9. The sample treated at 723

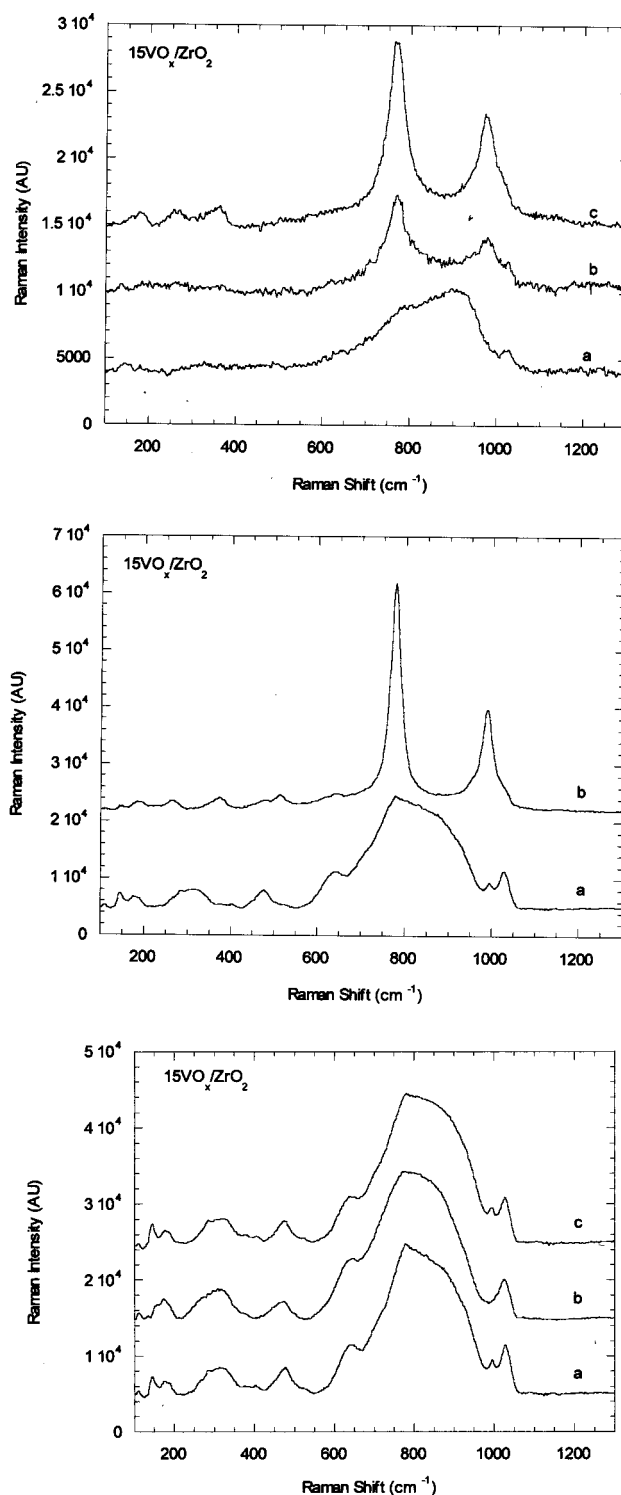


Figure 9. Raman spectra of 15VO_x/ZrO₂: (top) taken at (a) 723, (b) 823, and (c) 923 K; (middle) taken at 298 K after calcining at (a) 723 K and (b) 923 K. (bottom) taken at 298 K after (a) oxidation, (b) reduction, and (c) reoxidation at 723 K.

K shows a peak at 1028 cm⁻¹, indicative of monovanadate species, and a broad band from 700 to 980 cm⁻¹, indicative of polyvanadate species. After heating to 823 and 923 K, this broad band decreases in intensity, while two peaks at 778 and 977 cm⁻¹, attributed to ZrV₂O₇, appear.^{13,14} A shoulder at 1030 cm⁻¹ on the 977 cm⁻¹ peak suggests the presence of monovanadate species along with ZrV₂O₇. The changes seen in the Raman spectrum occur simultaneously with a sharp decrease in the surface area (Table 2).

Spectrum a in the middle panel of Figure 9 shows the $15\text{VO}_x/\text{ZrO}_2$ sample at 298 K after oxidation at 723 K. Peaks at 175, 330, 477, and 648 cm^{-1} indicate ZrO_2 in its tetragonal structure. Spectrum b in the same figure shows the $15\text{VO}_x/\text{ZrO}_2$ sample at 298 K after oxidation at 923 K. Peaks appear at 266 and 358 cm^{-1} , indicating the transition from tetragonal to monoclinic ZrO_2 .^{14,40} These results agree with Sohn et al., who reported ZrV_2O_7 formation at similar temperatures, along with the transition of ZrO_2 from its tetragonal to its monoclinic phase.¹⁵ The results here suggest that ZrV_2O_7 is formed by polyvanadate surface species interacting with ZrO_2 as it starts to form a monoclinic phase.

The UV–visible absorption edge for the ZrO_2 supported sample (Table 3) appears at 2.3 eV after oxidization at 723 K, with higher calcination temperatures leading to a slight decrease in the absorption edge energy. This suggests that formation of ZrV_2O_7 does not significantly alter the domain size of surface V^{5+} centers.

After oxidation at 723 K (100 cm^3/min of 10% O_2/He for 1 h), the ZrO_2 -supported sample was exposed to reduction (100 cm^3/min of 10% H_2/He for 2 h) and oxidation (100 cm^3/min of 10% O_2/He for 3 h) cycles at 723 K. Raman spectra of the sample taken in flowing He at 373 K after each treatment are shown in Figure 9, bottom panel. Upon reduction, peaks at 143 and 995 cm^{-1} are no longer present, indicating the reduction of V_2O_5 . Peaks for ZrO_2 and for monovanadate and polyvanadate species do not change upon reduction. After reoxidation, the two V_2O_5 peaks return to their original intensity, indicating that reduction and oxidation are entirely reversible in ZrO_2 -supported samples.

Reduction at 723 K does not influence the main absorption edge at 2.3 eV (Table 4). This behavior is consistent with that of the oxidation experiments; VO_4 -type species linked in polyvanadate domains retain their connectivity following reduction or formation of ZrV_2O_7 .

$9.4\text{VO}_x/\text{HfO}_2$ ($5.4\text{ VO}_x/\text{nm}^2$). Raman spectra of $9.4\text{VO}_x/\text{HfO}_2$ taken in flowing 10% O_2/He at 723, 823, and 923 K are shown in the top panel of Figure 10. At 723 and 823 K, a peak at 1027 cm^{-1} indicates the presence of monovanadate species, a broad band from 820 to 980 cm^{-1} indicates the presence of polyvanadate species, and a peak at 800 cm^{-1} is attributed to hafnium vanadate (HfV_2O_7).² At 923 K, three bands at 271, 380, and 510 cm^{-1} corresponding to monoclinic HfO_2 appear.⁴⁰ The Raman spectrum is dominated, however, by two sharp peaks at 800 and 993 cm^{-1} . Spectra taken at 298 K after treatment at 723 and 923 K are shown in Figure 10, middle panel, to illustrate the changes in VO_x/HfO_x structure induced by oxidation at higher temperature.

On the basis of the similarity between these results and those reported here for ZrV_2O_7 formation, it appears that the two peaks at 800 and 993 cm^{-1} are indicative of HfV_2O_7 , a compound isostructural with ZrV_2O_7 .⁴¹ Both ZrV_2O_7 and HfV_2O_7 exist in a NaCl cubic structure composed of M^{4+} and $\text{V}_2\text{O}_7^{4-}$ ions. In this structure, V^{5+} ions exist in tetrahedral coordination and M^{4+} ions exist in octahedral coordination.^{41,42} As with ZrV_2O_7 , the formation of HfV_2O_7 occurs concurrently with the transition of the support to its monoclinic phase, as evidenced by both Raman results and by the concurrent decrease in the surface area of these samples (Table 2). This would suggest that HfV_2O_7 and ZrV_2O_7 are formed via identical pathways.

The assignment of the two bands at 800 and 993 cm^{-1} to HfV_2O_7 is based on an analogy to the vibrational mode analysis of $\text{M}^{4+}\text{P}_2\text{O}_7^{4-}$ compounds published by Hubin and Tarte.⁴³

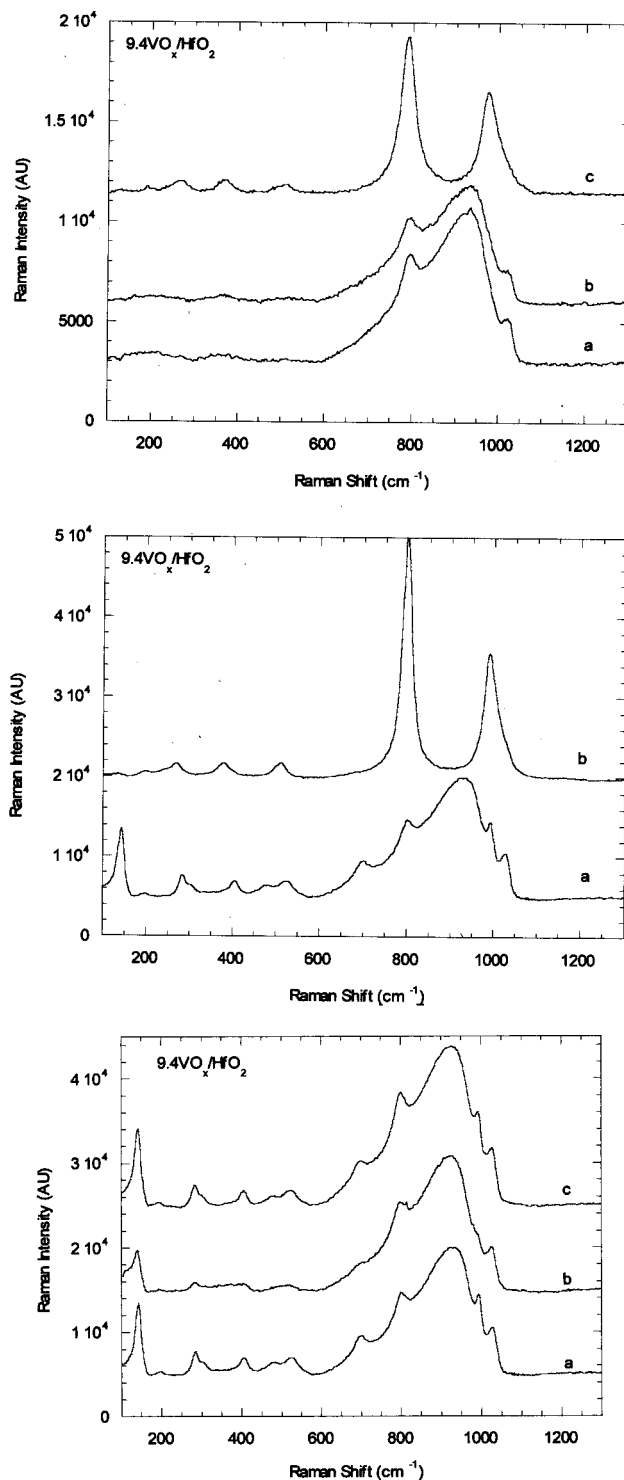


Figure 10. Raman spectra of $9.4\text{VO}_x/\text{HfO}_2$: (top) taken at (a) 723, (b) 823, and (c) 923 K; (middle) taken at 298 K after calcining at (a) 723 K and (b) 923 K; (bottom) taken at 298 K after (a) oxidation, (b) reduction, and (c) reoxidation at 723 K.

These authors analyzed $\text{M}^{4+}\text{P}_2\text{O}_7^{4-}$ compounds ($\text{M} = \text{Ti}, \text{Zr}, \text{Hf}$) to establish the effect of the metal cation on the internal vibrations of P_2O_7 . They found that the PO_3 vibration frequencies increased from 980 and 1116 cm^{-1} to 991 and 1132 cm^{-1} when M was changed from Zr to Hf . These shifts correspond very well with the shifts reported here for vanadate frequencies in ZrV_2O_7 and HfV_2O_7 . The lower of the two main bands shifts from 778 to 800 cm^{-1} while the higher band shifts from 977 to 993 cm^{-1} .

The UV–visible absorption edge energy for $9.4\text{VO}_x/\text{HfO}_2$ (Table 3) is present at 2.7 eV after oxidation at 723 K for 1 h. Higher oxidation temperatures lead to a decrease in the UV–visible absorption edge energy, perhaps due to a loss in surface area and the subsequent linking of VO_x surface groups.

After oxidation at 723 K (100 cm^3/min of 10% O_2/He for 1 h), a HfO_2 -supported sample was subject to reduction (100 cm^3/min of 10% H_2/He for 2 h) and oxidation (100 cm^3/min of 10% O_2/He for 3 h) cycles at 723 K. Raman spectra of the sample taken in flowing He at 373 K after each treatment are shown in the bottom panel of Figure 10. As with VO_x/ZrO_2 , reduction in H_2 leads to the disappearance of V_2O_5 peaks followed by their reappearance after reoxidation. There is no evidence of reduction of either HfO_2 or of the other vanadia species on the HfO_2 support, and the reduction does not alter the UV–visible absorption edge energy (Table 4).

Discussion

In agreement with previous reports,^{1,13,44} the structure of supported vanadia exposed to ambient air depends on the support material and on the VO_x surface density. On SiO_2 , the primary structures detected by Raman spectroscopy are crystalline V_2O_5 and very small amounts of polyvanadate species. The proportion of V_2O_5 grows with increasing vanadia surface density, as evidenced by both Raman spectroscopy and near-edge X-ray absorption spectroscopy (XANES). The absolute value of the UV–visible absorption edge energy is similar to that of V_2O_5 and approaches this value asymptotically as the surface density of vanadia increases. V_2O_5 crystallites, undetectable by X-ray diffraction at surface densities of 0.5 VO_x/nm^2 , line breadths corresponding to 30–40 nm as the surface density reaches 4.0 VO_x/nm^2 .

The structure of hydrated $\text{VO}_x/\text{Al}_2\text{O}_3$ also changes with VO_x surface density. At low surface densities (<1 VO_x/nm^2), polyvanadate species coexist with a small amount of V_2O_5 . As VO_x density increases, the structure of the dispersed vanadia resembles that detected on SiO_2 , the only difference being a somewhat higher concentration of polyvanadate species than on VO_x/SiO_2 . Consistent with this picture, the UV–visible absorption edge energy decreases with increasing vanadia surface density and asymptotically approaches that of V_2O_5 . In contrast, hydrated VO_x/TiO_2 , VO_x/ZrO_2 , and VO_x/HfO_2 are present primarily as polyvanadate species; on ZrO_2 and HfO_2 , they coexist with small amounts of V_2O_5 . Small amounts of ZrV_2O_7 and HfV_2O_7 are also evident in the samples of high surface density (>5 VO_x/nm^2) when vanadia is supported on ZrO_2 and HfO_2 .

Dehydration of supported vanadia results in several characteristic changes on all supports. The UV–visible absorption edge energy increases, consistent with a decrease in the average size of the vanadia domains and slight changes in the coordination of the vanadium cations. This effect is most pronounced for VO_x/SiO_2 and VO_x/TiO_2 , and for the higher density samples of VO_x/HfO_2 , but is relatively small for $\text{VO}_x/\text{Al}_2\text{O}_3$ and VO_x/ZrO_2 . Raman spectroscopy shows that in all cases a band at about 1030 cm^{-1} appears upon dehydration, characteristic of isolated monovanadate species. For SiO_2 and Al_2O_3 supported VO_x , Raman spectroscopy also reveals a decrease in the concentration of polyvanadate species relative to V_2O_5 . For vanadia dispersed on ZrO_2 and HfO_2 , however, the proportion of V_2O_5 appears to decrease relative to polyvanadate species upon dehydration of the samples, this trend being more pronounced for vanadia supported on HfO_2 .

The effects of dehydration on the structure of dispersed vanadia reported here can be interpreted in the following

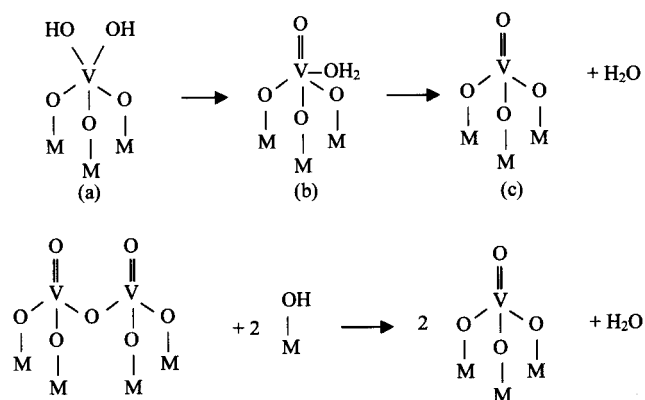


Figure 11. (top) Schematic representation of the dehydration of mono/polyvanadate species: (a) hydrated diol species; (b) water association; (c) dehydrated tetrahedral species. (bottom) Depolymerization of polyvanadate species upon dehydration.

manner. The appearance of a Raman band at 1030 cm^{-1} associated with $\text{V}=\text{O}$ stretching vibrations in monovanadate on all supports has been attributed to either dehydration of $\text{V}(\text{OH})_2$ species (Figure 11, top)^{8,11} or to depolymerization of polyvanadate species (Figure 11, middle).⁴ The latter process requires the participation of hydroxyl groups from the support surface, and it has been suggested that the stronger the basicity of these groups, the greater the extent of polyvanadate dehydration.⁴⁴ Consistent with this suggestion, we find that the extent of monovanadate formation at a nearly constant surface loading of vanadia decreases in the order $\text{HfO}_2 > \text{Al}_2\text{O}_3 > \text{ZrO}_2 > \text{TiO}_2 > \text{SiO}_2$. The observed decrease in polyvanadate Raman bands on SiO_2 and Al_2O_3 may be due to depolymerization of these species as proposed in Figure 11, middle panel. With the exception of VO_x/HfO_2 , there is little evidence of any change in the structure of crystalline V_2O_5 . In the case of VO_x/HfO_2 , the Raman spectra shown in Figure 5e indicate an increase in the concentration of polyvanadate species relative to V_2O_5 . In view of the strong similarity between ZrO_2 and HfO_2 , the difference in hydration effects between VO_x/ZrO_2 and VO_x/HfO_2 is unexpected.

Raman spectra taken during the oxidation of dispersed vanadia clearly show that the vanadia overlayer can undergo significant structural changes depending on the oxidation temperature and the composition of the support. For vanadia dispersed on SiO_2 and Al_2O_3 , the Raman features attributable to V_2O_5 crystallites disappear and new features appear as temperature increases from 723 to 923 K (Figures 6 and 7, top panels). While the highest calcination temperature (923 K) is below the melting point of bulk V_2O_5 (963 K), the temperature is above the Tamman temperature so that surface spreading of V_2O_5 is likely to occur. The exact structure or structures formed from the interactions of SiO_2 and Al_2O_3 with V_2O_5 are unclear, but it is reasonable to suggest that these may resemble individual sheets or partial sheets of V_2O_5 . Significant differences in the effects of support composition are observed though, when spectra are taken upon cooling VO_x/SiO_2 or $\text{VO}_x/\text{Al}_2\text{O}_3$ from 923 to 298 K (see Figures 6 and 7, middle panels). In the case of SiO_2 , the bands for V_2O_5 become more intense relative to that for monovanadate species. By contrast, the spectrum taken of $\text{VO}_x/\text{Al}_2\text{O}_3$ shows no evidence for V_2O_5 but only features that can be ascribed to mono- and polyvanadates. This suggests that on Al_2O_3 , high-temperature calcination results in the wetting of the support surface by two-dimensional sheets or ribbons of vanadia derived from V_2O_5 . Since vanadia does not wet SiO_2 , high-temperature calcination results only in the agglomeration of V_2O_5 into larger particles.

On TiO₂, polvanadate structures formed upon oxidation at 723 K remain stable up to 823 K, but at 923 K they appear to undergo some type of transformation since new Raman bands appear centered at 800 and 900 cm⁻¹. The intensity of the band at 900 cm⁻¹ decreases upon cooling from 923 to 298 K. The appearance of rutile TiO₂ bands confirms previous findings that surface vanadia migrates into titania and forms a rutile-vanadia compound.^{19,20} No evidence of V₂O₅ crystallites is observed.

Vanadia dispersed on ZrO₂ and HfO₂ occurs primarily in the form of polyvanadate species with evidence for only a small amount of ZrV₂O₇ or HfV₂O₇ (see Figures 9 and 10, middle panels). Oxidation at progressively higher temperatures eliminates the polyvanadate band and strongly increases the intensity of the (Zr/Hf)V₂O₇ bands. Upon cooling the sample following oxidation at 723 K, a very small amount of V₂O₅ is observed, but there is no change in the Raman spectrum observed upon cooling after treatment at 923 K.

Significant changes in the Raman spectrum of dispersed vanadia after reduction at 723 K in H₂ are evident only for VO_x/Al₂O₃. As seen in the bottom panel of Figure 7, H₂ reduction at 723 K has much the same effect as calcination at 823 K and higher. All traces of V₂O₅ disappear, and the only observable species are polyvanadates and monovanadates. It would, therefore, appear that the creation of anionic vacancies in V₂O₅ somehow facilitates the wetting of Al₂O₃. Reoxidation at 723 K restores some of the V₂O₅, but a noticeable amount of polyvanadate species remain. While the process by which H₂ reduction facilitates the spreading of V₂O₅ on Al₂O₃ is not understood, the surface rearrangement caused by reduction has significant catalytic implications. For the oxidative dehydrogenation of propane, VO_x/Al₂O₃ was found to be more selective and active than VO_x/SiO₂.² The spectra labeled a in the middle panels of Figures 6 and 7 indicate that freshly oxidized VO_x is found on both supports primarily as monovanadate and V₂O₅ species. Once reduced, however, the surface structures become significantly different as seen in the spectra labeled b in the bottom panels of Figures 6 and 7. The activation of C-H bonds in oxidative dehydrogenation reactions might induce a similar surface rearrangement and explain the high selectivity observed for VO_x/Al₂O₃ catalysts.² This interpretation of the similarity between reduction and oxidative dehydrogenation mechanisms would also explain the low activity and selectivity observed for catalysts with low VO_x coverage.² At low VO_x surface density, monovanadates are the most abundant surface species. The inability to reduce these species, as observed by Raman, might explain the low activity of monovanadates.

For ZrO₂ and HfO₂ supports, the only change in the Raman spectrum detected upon reduction in H₂ at 723 K is a loss of all V₂O₅ bands. These bands reappear, however, upon reoxidation of the samples at 723 K. It could be assumed that reduction of surface V₂O₅ produces polyvanadate species as it does on Al₂O₃, but no increase in polyvanadate bands is detected in the Raman spectra of reduced samples. A different explanation would be that V₂O₅ reduction forms color centers which give rise to strong absorption of the incident and scattered light in the reduced samples. Reoxidation would reverse this change and thereby restore V₂O₅ peaks.

The absence of any change in the structure of vanadia dispersed on ZrO₂ upon reduction presented here confirms recent reports by Su and Bell.¹⁴ It was shown that, at reduction temperatures up to 773 K, no change could be seen in the structure of the dispersed vanadia, consistent with the observa-

tion of very little oxygen removal from the oxide by either H₂ or C₃H₈. VO_x/HfO₂ catalysts behave in all respects to VO_x/ZrO₂.

Conclusions

Support composition and VO_x surface density influence the structure and behavior of supported VO_x catalysts. Following dehydration, all supports indicate the presence of monovanadate species at low weight loadings. These monovanadates tend to develop into larger-domain vanadia species as VO_x surface density increases. At high VO_x loading, vanadia exists predominantly as polyvanadate species on TiO₂, ZrO₂, and HfO₂, but as V₂O₅ on SiO₂ and Al₂O₃.

UV-visible and near-edge spectra indicate that supported VO_x species exist in larger domains and have higher-coordinate centers when hydrated. Dehydration consistently leads to a breakup of these domains. Raman spectra suggest that V=O bonds in mono- and polyvanadate species are most susceptible to hydration. On all supports, dehydration leads to the development of monovanadate species. Polyvanadate on TiO₂, ZrO₂, and HfO₂ also undergo structural changes when hydrated. Interpretation of this is more difficult because of the broad Raman bands which allow only qualitative assignments. Support material plays an important role in determining the extent of hydration, but this role might arise from the ability to support polymeric vanadia species.

Higher calcination temperatures produce significant changes in VO_x structure. On SiO₂, V₂O₅ sheets agglomerate, while on Al₂O₃, these same sheets transform into polyvanadate species. On ZrO₂ and HfO₂, a metal vanadate compound is formed. ZrV₂O₇ is formed at a lower temperature than HfV₂O₇, but the formation of both is accompanied by a decrease in surface area and a conversion of support phase, suggesting that both phases are formed as the support begins to transform into a monoclinic phase. Polyvanadate species form a mixed-metal species with rutile TiO₂.

H₂ reduction produces the most significant changes in VO_x/Al₂O₃, where surface V₂O₅ transitions into polyvanadate environments. On ZrO₂ and HfO₂, surface V₂O₅ is also reduced, but it is not clear what type of VO_x species results. Reduction of VO_x/TiO₂ leads to disappearance of monovanadate species. Reoxidation restores the original VO_x structures on SiO₂, ZrO₂, and HfO₂. On Al₂O₃, reoxidation does not progress to completion, perhaps because of kinetic limitations. Monovanadate species do not reappear on TiO₂ after reoxidation.

Acknowledgment. The authors wish to acknowledge T. D. Tilley for the provision of OV[OSi(O'Bu)₃]₃ and G. D. Meitzner for assistance in the interpreting X-ray near edge absorption data. This work was supported by the Director, Office of Basic Energy Sciences, Chemical Sciences Division, of the U.S. Department of Energy, under Contract DE-AC03-76SF00098. The authors acknowledge Stanford Synchrotron Radiation Laboratory and the U.S. Department of Energy for use of the beamline.

References and Notes

- (1) Bond, G. C.; Tahir, S. F. *Appl. Catal.* **1991**, *71*, 1.
- (2) Khodakov, A.; Olthof, B.; Bell, A. T.; Iglesia, E. *J. Catal.* **1999**, *181*, 205.
- (3) Wachs, I. E.; Weckhuysen, B. M. *Appl. Catal. A* **1997**, *157*, 67.
- (4) Went, G. T.; Oyama, S. T.; Bell, A. T. *J. Phys. Chem.* **1990**, *94*, 4240.
- (5) Eckert, H.; Wachs, I. E. *J. Phys. Chem.* **1989**, *93*, 6796.
- (6) Le Coustemer, L. R.; Taouk, B.; Le Meur, M.; Payen, E.; Guelton, M.; Grimblot, J. *J. Phys. Chem.* **1988**, *92*, 1230.

- (7) Morey, M.; Davidson, A.; Eckert, H.; Stucky, G. *Chem. Mater.* **1996**, *8*, 486.
- (8) Schraml-Marth, M.; Wokaun, A.; Pohl, M.; Krauss, H.-L. *J. Chem. Soc., Faraday Trans.* **1991**, *87*, 2635.
- (9) Das, N.; Eckert, H.; Hu, H.; Wachs, I. E.; Walzer, J. F.; Feher, F. *J. Phys. Chem.* **1993**, *97*, 8240.
- (10) Jehng, J.-M.; Deo, G.; Weckhuysen, B. M.; Wachs, I. E. *J. Mol. Catal. A* **1996**, *110*, 41.
- (11) Van Der Voort, P.; White, M. G.; Mitchell, M. B.; Verberckmoes, A. A.; Vasant, E. F. *Spectrochim. Acta A* **1997**, *53*, 2181.
- (12) Roozeboom, F.; Mittelmeijer-Hazeleger, M. C.; Moulijn, J. A.; Medema, J.; de Beer, V. H. J.; Gellings, P. J. *J. Phys. Chem.* **1980**, *84*, 2783.
- (13) Gao, X.; Bare, S. R.; Weckhuysen, B. M.; Wachs, I. E. *J. Phys. Chem.* **1998**, *102*, 10842.
- (14) Su, S.; Bell, A. T. *J. Phys. Chem.* **1998**, *102*, 7000.
- (15) Sohn, J. R.; Cho, S. G.; Pae, Y. I.; Hayashi, S. *J. Catal.* **1996**, *159*, 170.
- (16) El-Shobaky, G. A.; El-Nabarawy, K. A.; Abdalla, F. H. A. *Thermochim. Acta* **1985**, *96*, 129.
- (17) El-Shobaky, G. A.; El-Nabarawy, T.; Fagal, G. A.; Mokhtar, M. J. *Therm. Anal.* **1996**, *46*, 1473.
- (18) Briand, L. E.; Cornaglia, L.; Guida, J.; Thomas, H. J. *J. Mater. Chem.* **1995**, *5*, 1443.
- (19) Banares, M. A.; Alemany, L. J.; Jimenez, M. C.; Larrubia, M. A.; Delgado, F.; Granados, M. L.; Martinez-Arias, A.; Blasco, J. M.; Fierro, J. L. G. *J. Solid State Chem.* **1996**, *124*, 69.
- (20) Wachs, I. E.; Jehng, J. M.; Hardcastle, F. D. *Solid State Ionics* **1989**, *32/33*, 904.
- (21) Fournier, M.; Louis, C.; Che, M.; Chaquin, P.; Masure, D. *J. Catal.* **1989**, *119*, 400.
- (22) Weber, R. S. *J. Catal.* **1995**, *151*, 470.
- (23) Terry, K. W. Ph.D. Thesis, University of California, San Diego, CA, 1993.
- (24) Barton, D. G. Ph.D. Thesis, University of California, Berkeley, CA, 1998.
- (25) Lytle, F. W. In *Applications of Synchrotron Radiation*; Winick, H., Xian, D., Ye, M.-H., Huang, T., Eds.; Gordon and Breach Science Publishers: New York, 1988; p 135.
- (26) Barton, D. G.; Shtein, M.; Wilson, R. D.; Soled, S. L.; Iglesia, E. *J. Phys. Chem.*, submitted for publication.
- (27) Tauc, J. *Amorphous and Liquid Semiconductors*; Plenum: New York, 1974.
- (28) Benmoussa, M.; Ibnouelghazi, E.; Bennouna, A.; Ameziane, E. L. *Thin Solid Films* **1995**, *265*, 22.
- (29) Wong, J.; Lytle, F. W.; Messmer, R. P.; Maylotte, D. H. *Phys. Rev. B* **1984**, *30*, 5596.
- (30) Abello, L.; Husson, E.; Repelin, Y.; Lucazeau, G. *Spectrochim. Acta.* **1983**, *39A*, 641.
- (31) Beattie, I. R.; Gilson, T. R. *J. Chem. Soc. A* **1969**, 2322.
- (32) Busca, G.; Lavalley, J. C. *Spectrochim. Acta* **1986**, *42A*, 443.
- (33) Busca, G. *Mater. Chem. Phys.* **1988**, *19*, 157.
- (34) Hardcastle, F. D.; Wachs, I. E. *J. Phys. Chem.* **1991**, *95*, 5031.
- (35) Wachs, I. E. *Catal. Today* **1996**, *27*, 437.
- (36) Scharf, U.; Schraml-Marth, M.; Wokaun, A.; Baiker, A. *J. Chem. Soc., Faraday Trans.* **1991**, *87*, 3299.
- (37) Andersen, P. J.; Kung, H. H. *J. Phys. Chem.* **1992**, *96*, 3114.
- (38) Sobalik, Z.; Kozłowski, R.; Haber, J. *J. Catal.* **1991**, *127*, 665.
- (39) Went, G. T.; Leu, L. J.; Bell, A. T. *J. Catal.* **1992**, *134*, 479.
- (40) Anastassakis, E.; Papanicolaou, B.; Asher, I. M. *J. Phys. Chem. Solids* **1975**, *36*, 667.
- (41) Korthuis, V.; Khosrovani, N.; Sleight, A. W.; Roberts, N.; Dupree, R.; Warren, W. W. *Chem. Mater.* **1995**, *7*, 412.
- (42) Buchanan, R. C.; Wolter, G. W. *J. Electrochem. Soc. Solid State Sci. Technol.* **1983**, *130*, 1905.
- (43) Hubin, R.; Tarte, P. *Spectrochim. Acta* **1967**, *23A*, 1815.
- (44) Deo, G.; Wachs, I. E. *J. Phys. Chem.* **1991**, *95*, 5889.